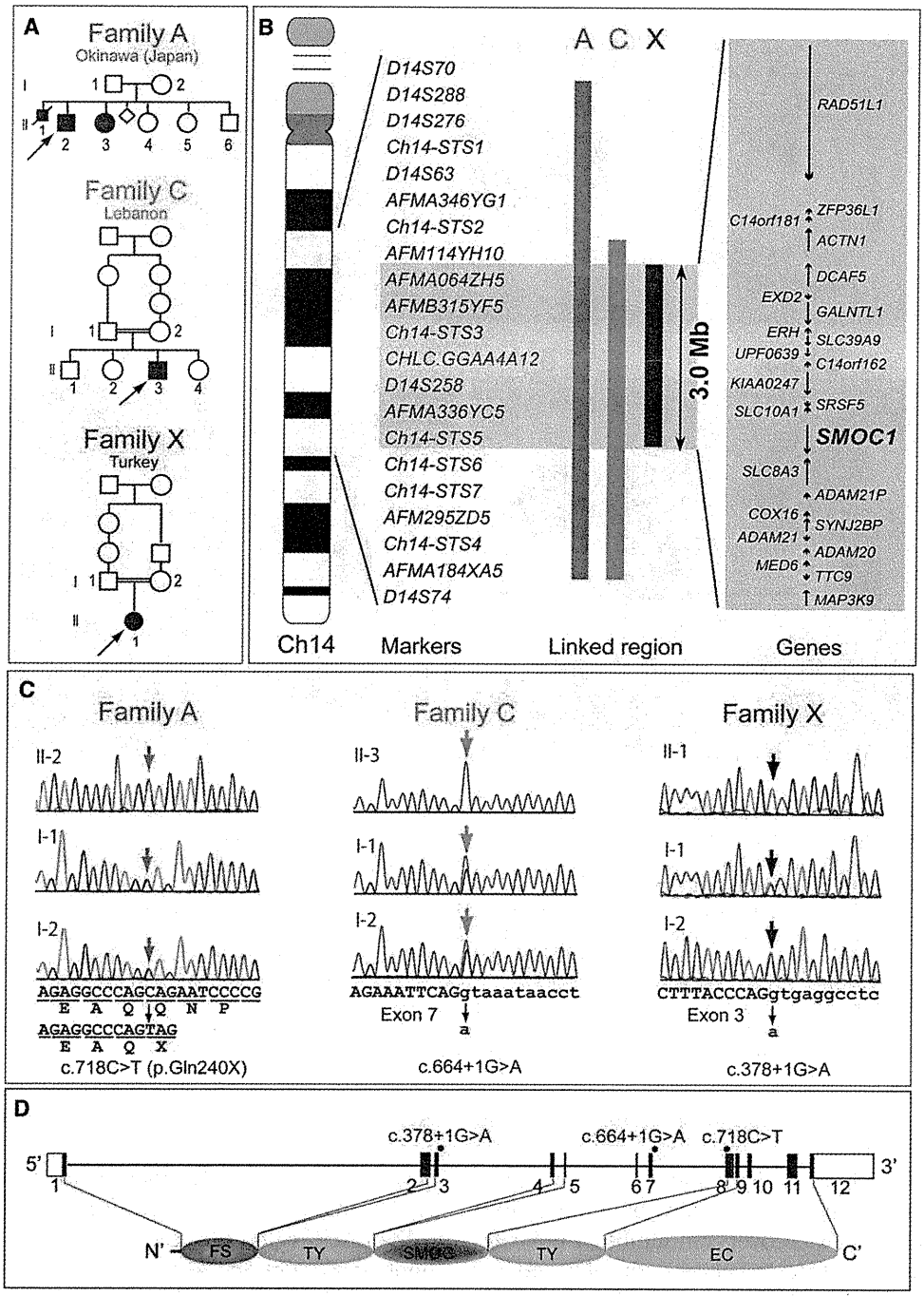

Figure 1. Genetic Analysis of Three Families with Members Affected by Microphthalmia with Limb Anomalies
(A) Pedigrees of the three families.
(B) Linkage analysis with SNPs and microsatellite markers on chromosome 14. From left to right: chromosome ideogram, genetic markers, linked regions of the three families, and genes mapped to the shortest overlapping linked region (between *AFM114YH10* and *Ch14-STS6* [UCSC coordinates, Feb. 2009: chromosome 14: 68,388,190–71,347,908 bp]).
(C) Sequences of mutations identified in each family. Affected patients in family A have a homozygous nonsense mutation (c.718C>T). Patients in families C and X have distinct homozygous splice-donor site mutations (c.664+1G>A and c.378+1G>A, respectively). For all mutations, parents of affected patients are heterozygous carriers, without exception. Sequences of the exon and intron are presented in upper and lower cases, respectively.
(D) At the top is a depiction of a schematic representation of *SMOC1* consisting of 12 exons (UTR and coding exons are indicated by open and filled rectangles, respectively). The locations of three mutations are indicated by red dots. At the bottom, the functional domains of SMOC1 are depicted. Abbreviations are as follows: FS, the follistatin-like domain; TY, the thyroglobulin-like domain; SMOC, the domain unique to SMOC; and EC, the extracellular calcium-binding domain.

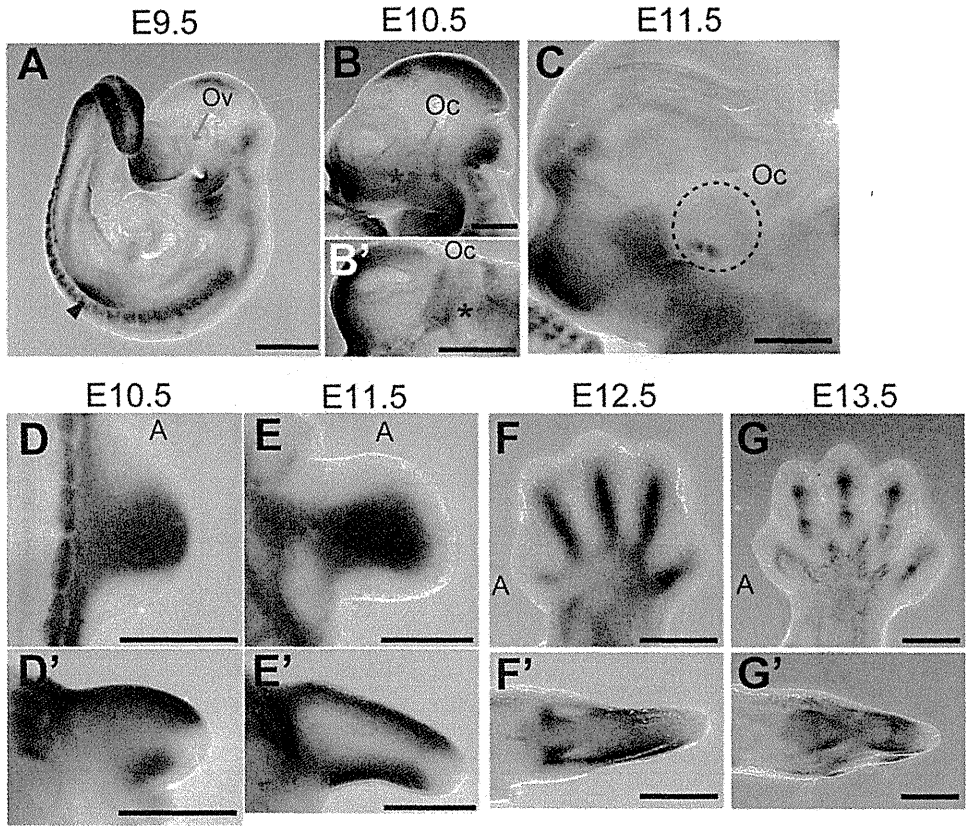

Figure 2. *Smoc1* Expression in Mouse Embryos
Lateral views of embryos (A–C) and a ventral view of the left part of the head (B′, lateral view is shown at the top).
(A) At E9.5, *Smoc1* was expressed in the forebrain, midbrain, hindbrain, pharyngeal arch, somites, and forelimb buds (magenta arrowhead), but not in the optic vesicle (Ov, blue arrow).
(B and B′) Expression in the optic stalk became evident at E10.5 (magenta asterisks), but was not evident in the optic cup (Oc, blue arrow).
(C) Expression was restricted to the closure site of the optic cup (dashed circle) at E11.5.
(D–G) Dorsal and (D′–G′) posterior view of the right hindlimbs (dorsal view is shown at the top in D′–G′). The anterior side is indicated by an A. (D and D′) At E10.5, *Smoc1* was more widely expressed in the dorsal part of the limb bud than in the ventral part. *Smoc1* expression is undetected in the most anterior, posterior, and distal parts of the limb bud. (E and E′) At E11.5, ventral expression was broader than that in the previous stage. (F and F′) At E12.5, expression was detected in areas consistent with chondrogenic condensation. (G and G′) At E13.5, *Smoc1* expression became restricted to future joint regions. Scale bar represents 500 μm.

tibia/fibula and calcanea of homozygous mice appeared malpositioned (Figures 4G and 4K), which might contribute to pes valgus. At P14, soft tissue syndactyly was also evident in most forelimbs of homozygous mice (Figures 4M–4O). Moreover, hindlimbs of homozygous mice showed synostosis between the 4^{th} and 5^{th} metatarsals (Figure 4T), which is observed in both the hands and the feet of MLA patients. Thus, many limb anomalies of MLA patients were recapitulated in *Smoc1* null mice (Table S1).

Reduced Interdigital Apoptosis and Disturbed BMP Signaling

Among the various abnormalities caused by loss of *Smoc1* function, we focused on soft tissue syndactyly, which was commonly observed in both fore- and hindlimbs of null mutants. It is possible that the syndactyly is caused by failed apoptotic regression of the interdigital mesenchyme. To examine this hypothesis, hindlimbs were stained with NB sulfate at E13.5 and E14.5, the time when interdigital apoptosis is most evident. In control embryos (WT and heterozygous littermates), NB-stained apoptotic cells were identified in the interdigital mesenchyme, where regression of the interdigital webbing occurs in the distal region (Figures 5A and 5C). By contrast, the number of apoptotic cells in the mesenchyme between digits 2 and 3 and digits 3 and 4 was dramatically reduced in homozygous mice at E13.5 and E14.5, along with persistent webbing in the distal region (Figures 5B and 5D, magenta asterisk). BMP signaling is involved in apoptosis of the interdigital mesenchyme.[25,26] *Bmp2*, *Bmp7*, and *Msx2*, a direct target of BMP signaling, were strongly expressed in the interdigital mesenchyme of control hindlimbs at both E12.5 and E13.5. However, the expression of these three genes was profoundly reduced and perturbed in hindlimbs of homozygous mice (Figures 5E–5J). These data suggest that inhibition of apoptosis is spatiotemporally correlated to reduced and/or disturbed expression of genes involved in BMP signaling in the interdigital mesenchyme.

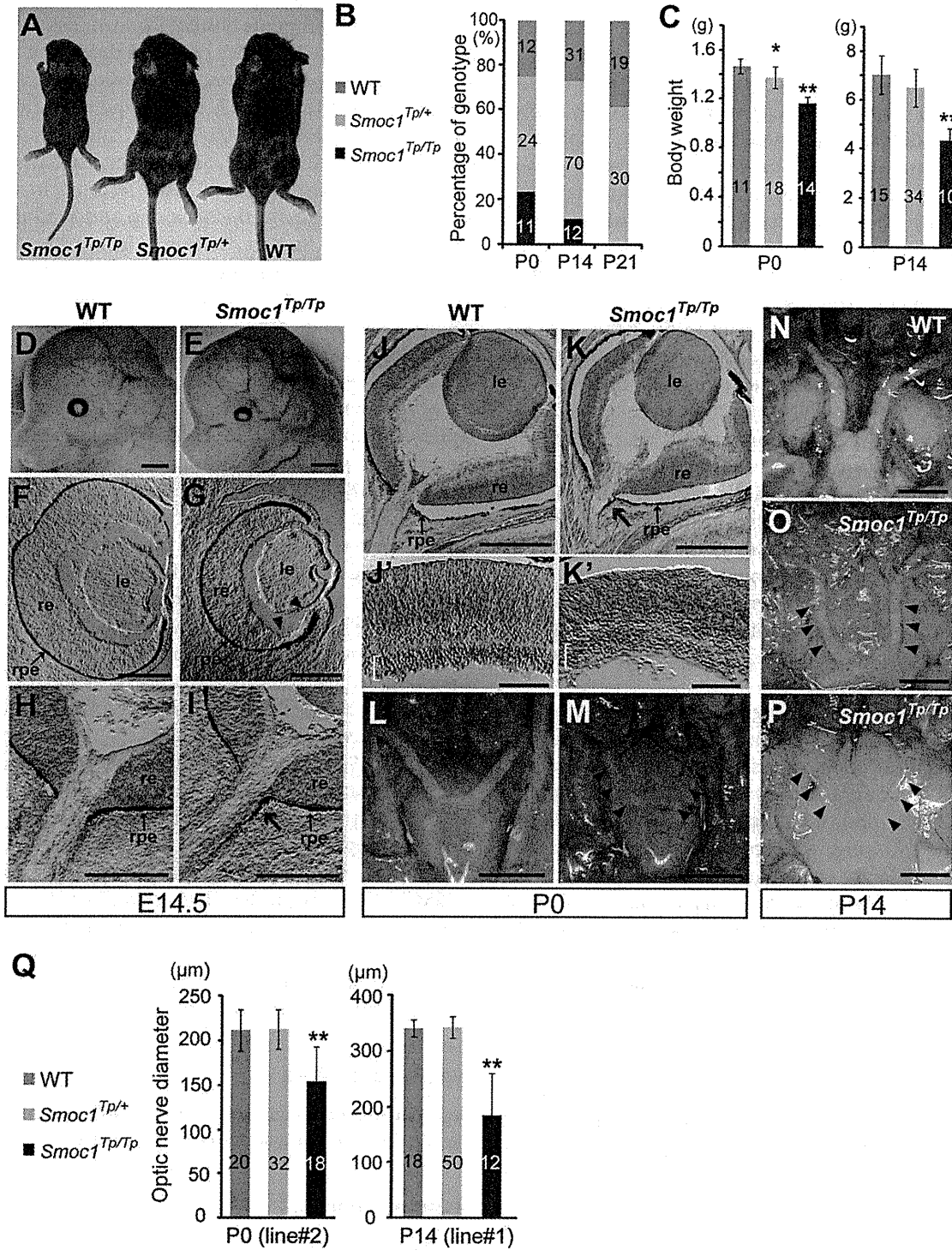

Figure 3. Growth and Ocular Phenotypes of *Smoc1* Null Mice

(A) Representative *Smoc1*$^{Tp/Tp}$ mouse, showing a small body in comparison to *Smoc1*$^{Tp/+}$ and WT littermates.

(B) Genotypes of living pups during the first 3 wk of life.

(C) Body weight of pups of each genotype at P0 (left panel) and P14 (right panel).

(D and E) Relatively small eyes were evident in *Smoc1*$^{Tp/Tp}$ mice in comparison to WT mice.

(F–K′) Coronal sections of eyes at E14.5 (F–I) and P0 (J–K′) with TB staining (H, I, and J–K′). (F-I) Atrophy of the anteroventral part of the retina (G, magenta arrowheads, dorsal view shown at the top), hypoplastic optic nerve, and extension of the RPE to the optic nerve (I, magenta arrow) in *Smoc1*$^{Tp/Tp}$ mice at E14.5. (J and K) Hypoplastic optic nerve and RPE extension in *Smoc1*$^{Tp/Tp}$ mice at P0 (K, magenta arrow). Note that sections in which optic nerves appeared most thick are presented in (H–K). (J′–K′) In higher-magnification views of (J and K), a thinned and irregular ganglion cell layer (white brackets) was observed in *Smoc1*$^{Tp/Tp}$ mice. Abbreviations are as follows: le, lens; re, retina; rpe, retinal pigmented epithelium.

(L–P) Ventral views of the brain showing optic nerves at P0 (L and M) and P14 (N–P), showing various degrees of optic nerve hypoplasia.

Discussion

In a previous report, we performed parametric linkage analysis with three families (families A, B, and C) and found 16 loci showing a LOD score ($\theta = 0.000$) higher than 3.0. Additional microsatellite markers highlighted only one locus, 10p11.23.[12] However, no mutations were found in the candidate gene *MPP7*.[12] By recruiting a new family (family X) to this study, we successfully found homozygous mutations in *SMOC1* in families A, C, and X. In family B, no *SMOC1* mutations were found, indicating the genetic heterogeneity in MLA. Patients with *SMOC1* mutations and *Smoc1* null mice showed similar limb anomalies, such as oligodactyly, syndactyly, synostosis of 4th and 5th metacarpals, hypoplasia of fibula, and bowed tibia. Oligodactyly, syndactyly, and synostosis of 4th and 5th metacarpals are common in MLA patients.[2–4] However, hypoplastic fibula and bowed tibia are less common in patients with MLA, as four out of 34 MLA patients showed these anomalies in the previous report.[3] Although one patient with a *SMOC1* mutation from family C did not show bowed tibia and hypoplastic fibula, these anomalies could be features specific to *SMOC1* mutations. Further *SMOC1* analysis of other MLA patients should delineate the phenotypic consequences caused by *SMOC1* mutations.

Accumulating evidence suggests that BMP signaling plays crucial roles in early eye vesicle and limb patterning, skeletal formation, and apoptosis of the interdigital mesenchyme,[25–29] and mutations involving BMP signaling cause human malformations including ocular, limb, and skeletal anomalies.[7,30–33] Here, we present genetic evidence that *SMOC1* is essential for ocular and limb development in humans and mice. Furthermore, *Xenopus smoc* can inhibit BMP signaling,[11] suggesting that *SMOC1/Smoc1* can also modulate BMP signaling in humans and mice. Indeed, we observed reduced and/or disturbed expression of genes involved in BMP signaling in the interdigital mesenchyme in *Smoc1* null mice, and limb and ocular abnormalities associated with loss of *Smoc1* function are consistent with phenotypic consequences of disturbed BMP signaling. Conditional inactivation of *Bmp2* in the limb showed 3/4 syndactyly, and a similar deficiency of both *Bmp2* and *Bmp7* resulted in malformed fibulae in mice.[25] Moreover, mice deficient in *Fmn1*, a repressor of BMP signaling, showed four digits, fused metatarsal bones, and an absence of fibulae in the hindlimbs,[34] suggesting the importance of altered BMP signaling in these features. Concerning ocular phenotypes, haploinsufficiency of mouse *Bmp4* resulted in a decreased number of ganglion layer cells and absence of the optic nerve similar to *Smoc1* null mice,[35] indicating that altered BMP signaling is also involved in the ocular phenotype. Interestingly, knockdown experiments of *smoc* by antisense morpholino in *Xenopus* showed absence or severe deformity of the eye and other anterior structures, which were accompanied by aberrant expression of *otx2*, *tbx2* in the eye field.[11] Mutations of *OTX2* (MIM 600037) cause micropthalmia, syndromic 5 (MCOPS5 [MIM 610125]) in humans.[36] Moreover, targeted disruption of *Tbx2* resulted in a marked reduction in the size of the optic cup and a failure of optic nerve formation in mice.[37] Thus, it is possible that loss of *SMOC1* function could alter the expression of *OTX2* and *TBX2* (MIM 600747) by disturbing BMP signaling in human developing eyes.

It is unknown how the loss of functional SMOC1, a BMP antagonist, leads to reduced expression of genes involved in BMP signaling in the interdigital mesenchyme in *Smoc1* null mice. In the case of *Fmn1*-deficient mice, the loss of the repressor of BMP signaling resulted in downregulation of *Fgf4* and *Shh* and in upregulation of *Gremlin* expression at E10.5, and absence of apoptosis of the interdigital mesenchyme between the two middle digits at E13.5.[34] Thus, there is a possibility that loss of SMOC1 could cause the imbalance among BMP, SHH, and FGF signaling, which would subsequently lead to reduced and/or disturbed expression of genes involved in BMP signaling in the interdigital mesenchyme. In fact, we observed reduced expression of *Msx2* in the progressive zone of hindlimbs at E11.5 (Figure S2). Moreover, expression of *Sox9*, the initial cartilage condensation marker, showed abnormal limb patterning, suggesting that SMOC1 may affect BMP signaling even at early stages of limb development (Figure S3). Further examinations are required for understanding spatial and temporal actions of SMOC1/Smoc1 protein during limb development.

In conclusion, our data demonstrate that *SMOC1/Smoc1* is an essential player in both ocular and limb development in humans and mice and give further support to the crucial roles of BMP signaling in these systems.

Supplemental Data

Supplemental Data include three figures and four tables and can be found with this article online at http://www.cell.com/AJHG/.

Acknowledgments

We would like to thank the patients and their families for their participation in this study. We thank Yoshiko Takahashi (Nara Institute of Science and Technology) and Atsushi Yamada (Showa University) for providing the *Bmp2* and *Sox9* probes; Elizabeth J. Robertson (University of Oxford) and Makoto Ishibashi (Kyoto University) for the *Bmp7* probe; Robert E. Maxson, Jr. (University of Southern California Keck School of Medicine) for the *Msx2*

(Q) Optic nerve diameter. Optic nerves were significantly hypoplastic in $Smoc1^{Tp/Tp}$ mice in comparison to WT and $Smoc1^{Tp/+}$ littermates. The numbers of pups (B and C) or eyes (Q) corresponding to each genotype are indicated within bars. Error bars indicate standard deviation: *$p < 0.01$, compared with WT. **$p < 0.01$, compared with WT and $Smoc1^{Tp/+}$. Scale bars represent 1 mm (D, E, and L–P), 200 μm (F–I), 500 μm (J and K), and 100 μm (J′ and K′).

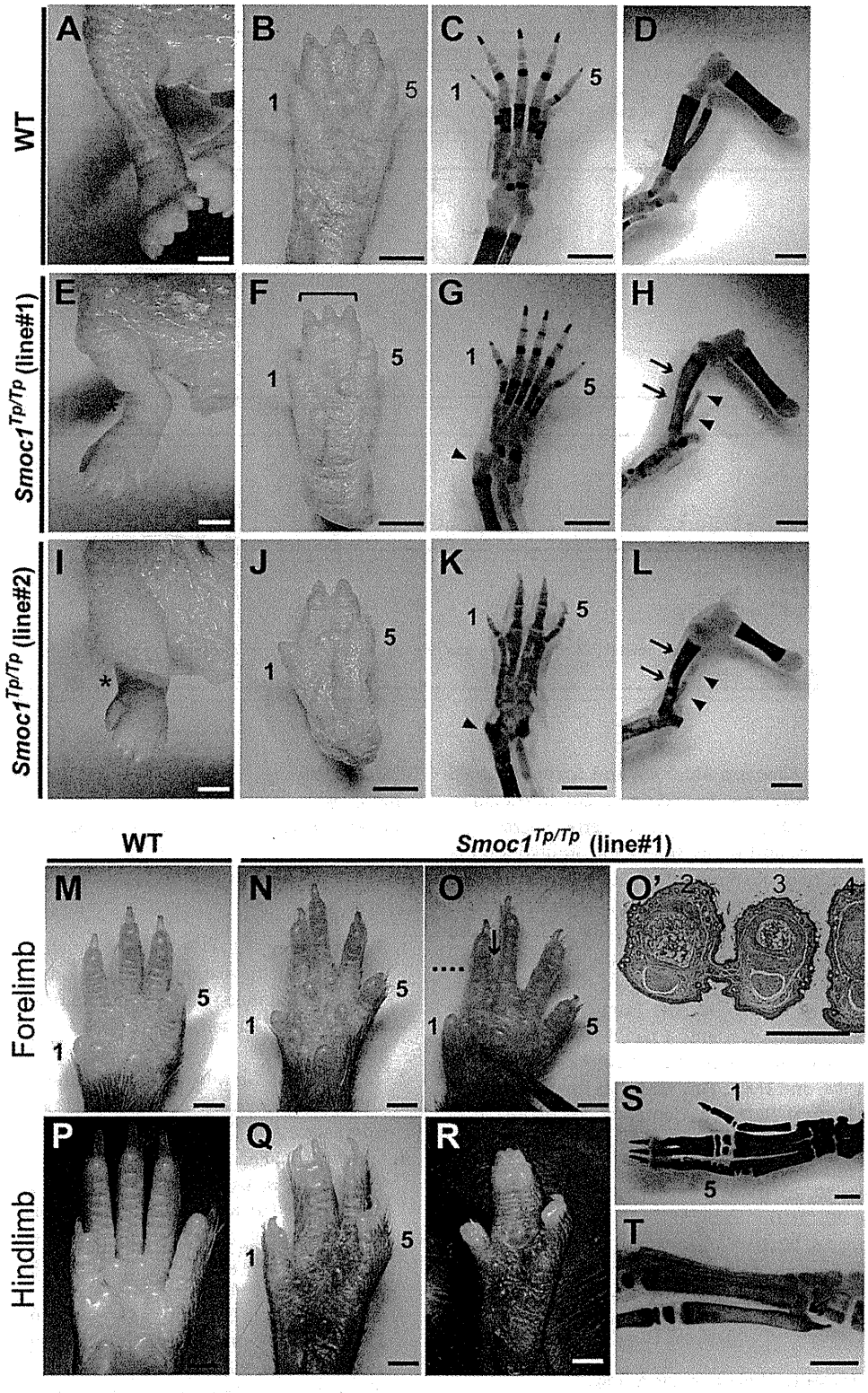

Figure 4. Limb Phenotypes of *Smoc1* Null Mice

Limbs of WT (A–D, M, and P) and *Smoc1*$^{Tp/Tp}$ mice (E–L, N–O′, and Q–T) at P0 (A–L) and P14 (M–T). Digit identities are indicated by the numbers 1 (thumb, anterior) and 5 (little finger, posterior). Skeletal staining with alcian blue and alizarin red is presented (C, D, G, H, K, L, S, and T). *Smoc1*$^{Tp/Tp}$ mice showed pes valgus (E and I), soft tissue syndactyly (F and G), and four digits with metatarsal fusion (J and K). Malposition of the articulation between the tibia/fibula and the calcanea (G and K, magenta arrowheads), bowed tibia (magenta arrows), and hypoplastic fibula (arrowheads) of *Smoc1*$^{Tp/Tp}$ mice (H and L) were observed. 2/3 soft tissue syndactyly (N) and 2/3 webbing (O) were evident in forelimbs of *Smoc1*$^{Tp/Tp}$ mice. (O′) A transverse section taken at the level indicated by the dashed line in (O) showed 2/3 webbing. 2/3 syndactyly (Q), 2/3/4 syndactyly (R), synostosis between the 2nd and 3rd proximal phalanx and metatarsals (S), and synostosis between the 4th and 5th metatarsals (T, arrow), observed in the hindlimbs of *Smoc1*$^{Tp/Tp}$ mice. Scale bars represent 1 mm (A–O and P–T) or 500 μm (O′).

Table 1. Limb Abnormalities in *Smoc1*$^{Tp/Tp}$ Mutants

Genotype	Talipes Valgus (No. of Affected/ Total No. of Pups)	Forelimb Abnormalities (No. of Limbs)	Hindlimb Syndactyly (No. of Limbs)					Other External Abnormalities (No. of Pups)	4th and 5th Metatarsal Fusion (No. of Affected/Total No. of Limbs)
			None	2/3[a]	3/4[b]	2/3/4[c]	4 Digits		
Postnatal Day 0									
Smoc1$^{Tp/+}$ (line 1, C57BL/6J)	0/42	0	84	0	0	0	0		
Smoc1$^{Tp/+}$ (line 2, ICR mixed)	0/38	0	76	0	0	0	0		
Smoc1$^{Tp/Tp}$ (line 1, C57BL/6J)	10/10	0	3	0	3	12	2		
Smoc1$^{Tp/Tp}$ (line 2, ICR mixed)	13/17	1[d]	1	1	9	4	19	cleft palate (3)	
Postnatal Day 14									
Smoc1$^{Tp/+}$ (line 1, C57BL/6J)	0/70	0	140	0	0	0	0		
Smoc1$^{Tp/Tp}$ (line 1, C57BL/6J)	11/11	18[e]	2	7	3	8	2	hypoplastic thumbs (5)	9/10[f]

[a] Syndactyly between the 2nd and 3rd digits.
[b] Syndactyly between the 3rd and 4th digits.
[c] Syndactyly between the 2nd, 3rd, and 4th digits.
[d] 2/3 soft tissue syndactyly.
[e] Eleven limbs showed 2/3 webbing, four limbs showed 2/3 soft tissue syndactyly, and one limb showed 3/4 syndactyly.
[f] Based on examination of skeletal preparations.

probe; Tomonori Hirose, Kazunori Akimoto, and Kazunori Sasaki (Yokohama City University) for providing useful information about mouse breeding, taking photos on a stereo microscope, and mRNA quantification; and Kohei Shiota and Sumiko Kimura (Kyoto University) for helpful comments about NB staining and limb anomalies. This work was supported by research grants from the Ministry of Health, Labour and Welfare (T. Furuichi, N. Miyake, N. Matsumoto, and H.S.) and the Japan Science and Technology Agency (N. Matsumoto), a Grant-in-Aid for Scientific Research from the Japan Society for the Promotion of Science (T. Furuichi and N. Matsumoto), and a Grant-in-Aid for Young Scientist from the Japan Society for the Promotion of Science (K.N., H.D., N. Miyake, and H.S.). This work has been carried out at the Advanced Medical Research Center of Yokohama City University.

Received: September 29, 2010
Revised: November 20, 2010
Accepted: November 26, 2010
Published online: December 30, 2010

Web Resources

The URLs for data presented herein are as follows:

BDGP, http://www.fruitfly.org/
ESEfinder 3.0, http://rulai.cshl.edu/cgi-bin/tools/ESE3/esefinder.cgi?process=home
GenBank, http://www.ncbi.nlm.nih.gov/Genbank/
HSF2.4.1, http://www.umd.be/HSF/
NetGene2, http://www.cbs.dtu.dk/services/NetGene2/
Online Mendelian Inheritance in Man, http://www.ncbi.nlm.nih.gov/Omim
UCSC Genome Browser, http://genome.ucsc.edu/cgi-bin/hgGateway
SpliceView, http://zeus2.itb.cnr.it/~webgene/wwwspliceview.html

References

1. Waardenburg, P.J. (1961). Autosomally-recessive anophthalmia with malformations of the hands and feet. In Genetics and Ophthalmology, P.J. Waardenburg, A. Franceschetti, and D. Klein, eds. (Assen, The Netherlands: Royal Van Gorcum), p. 773.
2. Teiber, M.L., Garrido, J.A., and Barreiro, C.Z. (2007). Ophthalmo-acromelic syndrome: report of a case with vertebral anomalies. Am. J. Med. Genet. A. *143A*, 2460–2462.
3. Garavelli, L., Pedori, S., Dal Zotto, R., Franchi, F., Marinelli, M., Croci, G.F., Bellato, S., Ammenti, A., Virdis, R., Banchini, G., and Superti-Furga, A. (2006). Anophthalmos with limb anomalies (Waardenburg opththalmo-acromelic syndrome): report of a new Italian case with renal anomaly and review. Genet. Couns. *17*, 449–455.
4. Tekin, M., Tutar, E., Arsan, S., Atay, G., and Bodurtha, J. (2000). Ophthalmo-acromelic syndrome: report and review. Am. J. Med. Genet. *90*, 150–154.
5. Adler, R., and Canto-Soler, M.V. (2007). Molecular mechanisms of optic vesicle development: complexities, ambiguities and controversies. Dev. Biol. *305*, 1–13.
6. Zeller, R., López-Ríos, J., and Zuniga, A. (2009). Vertebrate limb bud development: moving towards integrative analysis of organogenesis. Nat. Rev. Genet. *10*, 845–858.
7. Bakrania, P., Efthymiou, M., Klein, J.C., Salt, A., Bunyan, D.J., Wyatt, A., Ponting, C.P., Martin, A., Williams, S., Lindley, V., et al. (2008). Mutations in BMP4 cause eye, brain, and digit

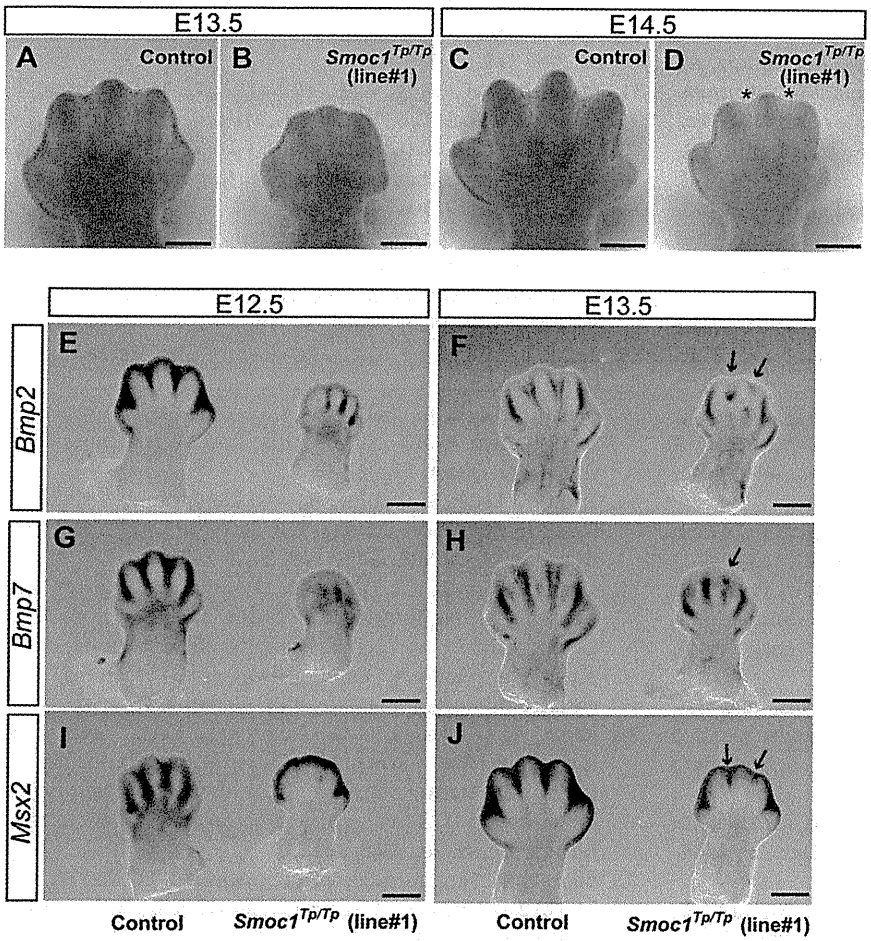

Figure 5. Reduced Apoptosis and Altered BMP Signaling in the Interdigital Mesenchyme of *Smoc1* Null Mice

(A–D) NB staining of left hindlimbs at E13.5 (A and B) and E14.5 (C and D). In comparison to control embryos (WT and $Smoc1^{Tp/+}$ littermates) (A and C), the number of NB-stained apoptotic cells in the interdigital mesenchyme of $Smoc1^{Tp/Tp}$ mice was dramatically reduced between digits 2 and 3 and digits 3 and 4 at both E13.5 and E14.5, and the webbing remained at a distal level (B and D, magenta asterisk).

(E–J) Whole-mount in situ hybridization of right hindlimbs at E12.5 (E, G, and I) and E13.5 (F, H, and J). At E12.5, interdigital expression of *Bmp2*, *Bmp7*, and *Msx2* was profoundly delayed in the hindlimbs of $Smoc1^{Tp/Tp}$ mice, and their expression in the interdigital mesenchyme was apparently perturbed, even at E13.5 (magenta arrows). Scale bar represents 500 μm.

developmental anomalies: overlap between the BMP4 and hedgehog signaling pathways. Am. J. Hum. Genet. *82*, 304–319.

8. Bornstein, P., and Sage, E.H. (2002). Matricellular proteins: extracellular modulators of cell function. Curr. Opin. Cell Biol. *14*, 608–616.
9. Vannahme, C., Smyth, N., Miosge, N., Gösling, S., Frie, C., Paulsson, M., Maurer, P., and Hartmann, U. (2002). Characterization of SMOC-1, a novel modular calcium-binding protein in basement membranes. J. Biol. Chem. *277*, 37977–37986.
10. Gersdorff, N., Müller, M., Schall, A., and Miosge, N. (2006). Secreted modular calcium-binding protein-1 localization during mouse embryogenesis. Histochem. Cell Biol. *126*, 705–712.
11. Thomas, J.T., Canelos, P., Luyten, F.P., and Moos, M., Jr. (2009). Xenopus SMOC-1 inhibits BMP signaling downstream of receptor binding and is essential for post-gastrulation development in Xenopus. J. Biol. Chem. *284*, 18994–19005.
12. Hamanoue, H., Megarbane, A., Tohma, T., Nishimura, A., Mizuguchi, T., Saitsu, H., Sakai, H., Miura, S., Toda, T., Miyake, N., et al. (2009). A locus for ophthalmo-acromelic syndrome mapped to 10p11.23. Am. J. Med. Genet. A. *149A*, 336–342.
13. Mégarbané, A., Souraty, N., and Tamraz, J. (1998). Ophthalmo-acromelic syndrome (Waardenburg) with split hand and polydactyly. Genet. Couns. *9*, 195–199.
14. Cogulu, O., Ozkinay, F., Gündüz, C., Sapmaz, G., and Ozkinay, C. (2000). Waardenburg anophthalmia syndrome: report and review. Am. J. Med. Genet. *90*, 173–174.
15. Miyake, N., Kosho, T., Mizumoto, S., Furuichi, T., Hatamochi, A., Nagashima, Y., Arai, E., Takahashi, K., Kawamura, R., Wakui, K., et al. (2010). Loss-of-function mutations of CHST14 in a new type of Ehlers-Danlos syndrome. Hum. Mutat. *31*, 966–974.
16. Gudbjartsson, D.F., Thorvaldsson, T., Kong, A., Gunnarsson, G., and Ingolfsdottir, A. (2005). Allegro version 2. Nat. Genet. *37*, 1015–1016.
17. Keng, V.W., Yae, K., Hayakawa, T., Mizuno, S., Uno, Y., Yusa, K., Kokubu, C., Kinoshita, T., Akagi, K., Jenkins, N.A., et al. (2005). Region-specific saturation germline mutagenesis in mice using the Sleeping Beauty transposon system. Nat. Methods *2*, 763–769.
18. Mamo, S., Gal, A.B., Bodo, S., and Dinnyes, A. (2007). Quantitative evaluation and selection of reference genes in mouse oocytes and embryos cultured in vivo and in vitro. BMC Dev. Biol. *7*, 14.
19. Parr, B.A., Shea, M.J., Vassileva, G., and McMahon, A.P. (1993). Mouse Wnt genes exhibit discrete domains of expression in the early embryonic CNS and limb buds. Development *119*, 247–261.
20. Saitsu, H., Ishibashi, M., Nakano, H., and Shiota, K. (2003). Spatial and temporal expression of folate-binding protein 1 (Fbp1) is closely associated with anterior neural tube closure in mice. Dev. Dyn. *226*, 112–117.
21. Tamplin, O.J., Kinzel, D., Cox, B.J., Bell, C.E., Rossant, J., and Lickert, H. (2008). Microarray analysis of Foxa2 mutant mouse embryos reveals novel gene expression and inductive roles

for the gastrula organizer and its derivatives. BMC Genomics *9*, 511.

22. Suzuki, D., Yamada, A., Amano, T., Yasuhara, R., Kimura, A., Sakahara, M., Tsumaki, N., Takeda, S., Tamura, M., Nakamura, M., et al. (2009). Essential mesenchymal role of small GTPase Rac1 in interdigital programmed cell death during limb development. Dev. Biol. *335*, 396–406.
23. Kimura, S., and Shiota, K. (1996). Sequential changes of programmed cell death in developing fetal mouse limbs and its possible roles in limb morphogenesis. J. Morphol. *229*, 337–346.
24. Sernagor, E., Eglen, S.J., and Wong, R.O. (2001). Development of retinal ganglion cell structure and function. Prog. Retin. Eye Res. *20*, 139–174.
25. Bandyopadhyay, A., Tsuji, K., Cox, K., Harfe, B.D., Rosen, V., and Tabin, C.J. (2006). Genetic analysis of the roles of BMP2, BMP4, and BMP7 in limb patterning and skeletogenesis. PLoS Genet. *2*, e216.
26. Robert, B. (2007). Bone morphogenetic protein signaling in limb outgrowth and patterning. Dev. Growth Differ. *49*, 455–468.
27. Dudley, A.T., Lyons, K.M., and Robertson, E.J. (1995). A requirement for bone morphogenetic protein-7 during development of the mammalian kidney and eye. Genes Dev. *9*, 2795–2807.
28. Khokha, M.K., Hsu, D., Brunet, L.J., Dionne, M.S., and Harland, R.M. (2003). Gremlin is the BMP antagonist required for maintenance of Shh and Fgf signals during limb patterning. Nat. Genet. *34*, 303–307.
29. Furuta, Y., and Hogan, B.L. (1998). BMP4 is essential for lens induction in the mouse embryo. Genes Dev. *12*, 3764–3775.
30. Asai-Coakwell, M., French, C.R., Berry, K.M., Ye, M., Koss, R., Somerville, M., Mueller, R., van Heyningen, V., Waskiewicz, A.J., and Lehmann, O.J. (2007). GDF6, a novel locus for a spectrum of ocular developmental anomalies. Am. J. Hum. Genet. *80*, 306–315.
31. Tassabehji, M., Fang, Z.M., Hilton, E.N., McGaughran, J., Zhao, Z., de Bock, C.E., Howard, E., Malass, M., Donnai, D., Diwan, A., et al. (2008). Mutations in GDF6 are associated with vertebral segmentation defects in Klippel-Feil syndrome. Hum. Mutat. *29*, 1017–1027.
32. Wyatt, A.W., Osborne, R.J., Stewart, H., and Ragge, N.K. (2010). Bone morphogenetic protein 7 (BMP7) mutations are associated with variable ocular, brain, ear, palate, and skeletal anomalies. Hum. Mutat. *31*, 781–787.
33. Ye, M., Berry-Wynne, K.M., Asai-Coakwell, M., Sundaresan, P., Footz, T., French, C.R., Abitbol, M., Fleisch, V.C., Corbett, N., Allison, W.T., et al. (2010). Mutation of the bone morphogenetic protein GDF3 causes ocular and skeletal anomalies. Hum. Mol. Genet. *19*, 287–298.
34. Zhou, F., Leder, P., Zuniga, A., and Dettenhofer, M. (2009). Formin1 disruption confers oligodactylism and alters Bmp signaling. Hum. Mol. Genet. *18*, 2472–2482.
35. Chang, B., Smith, R.S., Peters, M., Savinova, O.V., Hawes, N.L., Zabaleta, A., Nusinowitz, S., Martin, J.E., Davisson, M.L., Cepko, C.L., et al. (2001). Haploinsufficient Bmp4 ocular phenotypes include anterior segment dysgenesis with elevated intraocular pressure. BMC Genet. *2*, 18.
36. Ragge, N.K., Brown, A.G., Poloschek, C.M., Lorenz, B., Henderson, R.A., Clarke, M.P., Russell-Eggitt, I., Fielder, A., Gerrelli, D., Martinez-Barbera, J.P., et al. (2005). Heterozygous mutations of OTX2 cause severe ocular malformations. Am. J. Hum. Genet. *76*, 1008–1022.
37. Behesti, H., Papaioannou, V.E., and Sowden, J.C. (2009). Loss of Tbx2 delays optic vesicle invagination leading to small optic cups. Dev. Biol. *333*, 360–372.

CLINICAL REPORT

AMERICAN JOURNAL OF medical genetics PART A

A De Novo Deletion of 20q11.2–q12 in a Boy Presenting With Abnormal Hands and Feet, Retinal Dysplasia, and Intractable Feeding Difficulty

Yoko Hiraki,[1,2] Akira Nishimura,[2] Michiko Hayashidani,[3] Yoshiko Terada,[4] Gen Nishimura,[5] Nobuhiko Okamoto,[6] Sachiko Nishina,[7] Yoshinori Tsurusaki,[2] Hiroshi Doi,[2] Hirotomo Saitsu,[2] Noriko Miyake,[2] and Naomichi Matsumoto[2]*

[1]Hiroshima Municipal Center for Child Health and Development, Hiroshima, Japan

[2]Department of Human Genetics, Yokohama City University Graduate School of Medicine, Yokohama, Japan

[3]Medical Center for Premature and Neonatal Infants, Hiroshima City Hospital, Hiroshima, Japan

[4]Department of Ophthalmology, Hiroshima City Hospital, Hiroshima, Japan

[5]Department of Pediatric Imaging, Tokyo Metropolitan Children's Medical Center, Tokyo, Japan

[6]Department of Medical Genetics, Osaka Medical Center and Research Institute for Maternal and Child Health, Osaka, Japan

[7]Department of Ophthalmology, National Center for Child Health and Development, Tokyo, Japan

Received 18 June 2010; Accepted 23 October 2010

Proximal interstitial deletions involving 20q11–q12 are very rare. Only two cases have been reported. We describe another patient with 20q11.21–q12 deletion. We precisely mapped the 6.5-Mb deletion and successfully determined the deletion landmarks at the nucleotide level. Common clinical features among the three cases include developmental delay, intractable feeding difficulties with gastroesophageal reflux, and facial dysmorphism including triangular face, hypertelorism, and hypoplastic alae nasi, indicating that the 20q11.2–q12 deletion can be a clinically recognizable syndrome. This is also supported by the fact that the three deletions overlap significantly. In addition, unique features such as arthrogryposis/fetal akinesia (hypokinesia) deformation and retinal dysplasia are recognized in the patient reported herein. © 2011 Wiley-Liss, Inc.

Key words: 20q interstitial deletion; abnormal hands and feet; retinal dysplasia; feeding difficulty

How to Cite this Article:
Hiraki Y, Nishimura A, Hayashidani M, Terada Y, Nishimura G, Okamoto N, Nishina S, Tsurusaki Y, Doi H, Saitsu H, Miyake N, Matsumoto N. 2011. A de novo deletion of 20q11.2–q12 in a boy presenting with abnormal hands and feet, retinal dysplasia, and intractable feeding difficulty.
Am J Med Genet Part A 155:409–414.

INTRODUCTION

Interstitial deletions of the long arm of chromosome 20 are rare. To our knowledge, a total of 12 patients have been reported in the literature [Petersen et al., 1987; Shabtai et al., 1993; Aldred et al., 2002; Genevieve et al., 2005; Callier et al., 2006; Borozdin et al., 2007; Iqbal and Al-Owain, 2007]. Among them, only two cases showed the proximal q deletion (20q11–q12), not extending to q13 [Callier et al., 2006; Iqbal and Al-Owain, 2007]. One patient had a 6.6-Mb deletion at 20q11.21–q11.23 [Callier et al., 2006], and the other [Iqbal and Al-Owain, 2007] showed a 6.8-Mb deletion at 20q11.2–q12. Here, we report on the third patient with a 6.5-Mb deletion at 20q11.21–q12, clinically showing mental retardation, minor craniofacial anomalies, and intractable feeding difficulties. The deletion has been precisely analyzed at the nucleotide level and his detailed clinical manifestations will be presented.

Grant sponsor: Japan Society for the Promotion of Science (JSPS); Grant sponsor: Ministry of Health, Labour and Welfare; Grant sponsor: Ministry of Education, Culture, Sports, Science and Technology of Japan; Grant sponsor: Scientific Research.

*Correspondence to:
Naomichi Matsumoto, Department of Human Genetics, Yokohama City University Graduate School of Medicine, Fukuura 3-9, Kanazawa-ku, Yokohama 236-0004, Japan. E-mail: naomat@yokohama-cu.ac.jp

Published online 11 January 2011 in Wiley Online Library (wileyonlinelibrary.com).
DOI 10.1002/ajmg.a.33818

© 2011 Wiley-Liss, Inc.

CLINICAL REPORT

The 18-month-old boy was the first product of healthy 22-year-old mother and 25-year-old father without any consanguinity. Pregnancy was uneventful. Family history was unremarkable. He was born by spontaneous vaginal delivery at 38 weeks of gestation. Birth weight was 2,230 g (−1.7 SD), length 44.0 cm (−1.9 SD), and OFC 32.5 cm (−0.3 SD). Multiple malformations including patent ductus arteriosus, patency of foramen ovale, and dysmorphic face were noted. He was tube-fed due to poor swallowing and oxygen therapy was required until 4 months because of respiratory disturbance. X-ray examination at age of 1 month revealed small thorax and mild slender long bones. In addition, right eye retinal fold was pointed out. At age of 3 months, upper gastrointestinal tract was investigated because of recurrent vomiting, and gastroesophageal reflux (GER) and esophageal hiatus hernia were found. Esophageal hiatus hernia was alleviated spontaneously, but GER persisted.

At age of 4 months, he was referred to us for evaluation of his developmental delay. He was noted to have the following craniofacial features: triangular face, premature closure fontanelle, slopping forehead, wide bending eyebrows, hypertelorism, low-set and posterior rotated ears, long columella nasi, mild hypoplastic alae nasi, short and well-defined philtrum, thin lips with tucked-in lower lip, submucosal cleft palate, microretrognathia and posterior low hair-line (Fig. 1A,B and Table I). Additionally, abnormal hands and feet were recognized, consisted of restriction of all proximal interphalangeal joints and over-extension of all distal interphalangeal joints of hands and feet, radial deviation of 2nd fingers, clinodactyly of the 2nd and 5th fingers, lack of flexion creases bilaterally, right preaxial polydactyly, left single palmar, and talipes valgus. Mild restriction of elbow, hip and knee joints bilaterally was also noted (Fig. 1C–E and Table I).

At 15 months, his weight was 7.5 kg (−2.3 SD), length 71.8 cm (−2.7 SD), and OFC 44.4 cm (−1.6 SD). He could roll over one side and shift a toy from one hand to the other. Social smile was seen, but he could not recognize his parents (DQ 48). His dysphagia persisted based on the modified swallowing study [Kanda et al., 2005]; he required tube-feeding, and rejected oral intake. Ophthalmic examination at 15 months revealed broom-like pattern of retinal vessels extending from optic disc to periphery with a falciform retinal fold in the right eye, causing visual impairment. In the left eye, mild opacity in the lateral portion of vitreous body was found. These findings led to the diagnosis of bilateral retinal dysplasia. Anterior segment and optic disc were normal. Left hearing loss was suspected by auditory brainstem response, otoacoustic emission, and behavioral observation audiometry. Brain magnetic resonance imaging revealed cortical atrophy and mild ventriculomegaly. Blood biochemistry and abdominal ultrasonographic examination were all normal. Serological TORCH (toxoplasma, rubella, cytomegarovirus, and herpes simplex) testing was negative. At 18 months, the shortening of 5th middle phalanges of fingers and absence of middle phalanges of the toes were confirmed by X-ray examination.

CYTOGENETIC AND MOLECULAR ANALYSIS

G-banded chromosomal analysis (550 bands level) of the patient's blood lymphocytes indicated normal karyptype (46,XY) (data not shown). Fluorescence in situ hybridization (FISH) analysis using all

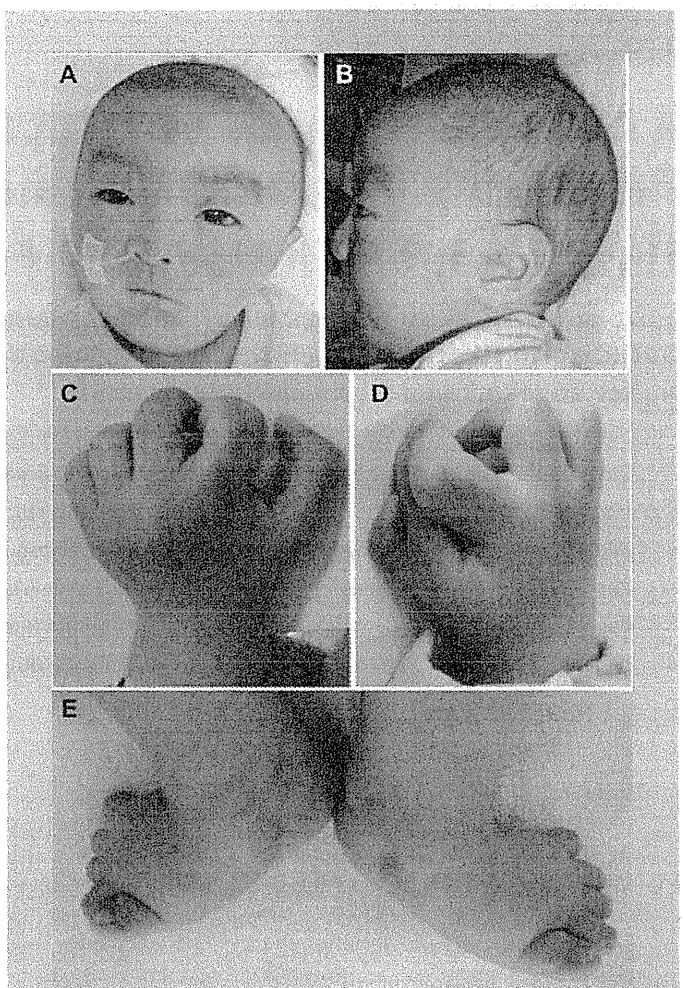

FIG. 1. Photographs of the patient at age of 4 months. A,B: Facial abnormalities including triangular face, wide and bending eyebrows, hypertelorism, long columella, thin lips with tucked-in lower lip, and microretrognathia were recognized. C (left hand) and D (right): Bilateral camptodactyly associated with radial deviation of the 2nd fingers and clinodactyly of the 2nd and 5th, and right preaxial polydactyly were noted. E: Camptodactyly with talipes valgus in both feet.

chromosomal subtelomeric clones did not show any abnormalities. Array CGH analysis using NimbleGen 385K Array (Roche NimbleGen, Inc., Madison, WI) demonstrated a 6.5-Mb heterozygous deletion at 20q11.2–q12 (UCSC genome coordinates 2006 Mar. version, chromosome 20: 31,269,661–37,782,841 bp) (Fig. 2A). The deletion was also confirmed by FISH using BACs (RP11-322B6 and RP11-782C16 at 21q11.21, and RP11-54P22 and RP11-467J15 at 20q12), RP11-787C16 and RP11-54P22 was deleted while RP11-322B6 and RP11-467J15 were not deleted (Fig. 3). The deletion junction was successfully amplified by PCR using primers (Primer A: 5′-TGA TAG AGC CAA CTG GGT CAT GTG C-3′, Primer C: 5′-TCT AGC TTG CTG AAT TCC TGC CTG A-3′) (Fig. 2B) and its product was sequenced. The deleted region was from 31,274,015 to 37,783,826 bp (6,509,811 bp) with 5-bp overlap (ATAGA) (Fig. 2C). The deletion occured de novo as FISH and

TABLE I. Clinical Manifestations of Reported Cases of 20q11–q12 Deletion

	Calliers' case (4 y, female)	Iqbals' case (2 y, male)	Present case (18 m, male)
General			
Growth retardation	+	+	+
Developmental delay	+	+	+
Autistic behavior	+	+	+
Sensory abnormalities/self-injury	+	+	+
Feeding difficulties	+	+	+
Gastroesophageal reflux	+	+	+
Gastrointestinal abnormalities	+ (Pyloric stenosis)	−	+ (Esophageal hiatus hernia)
Feeding intolerance	+ (Diarrhea, vomiting)	−	−
Dysphagia			+
Food refusal	+		+
Muscle tone	Hypertonia	Normal tone except for difficulty in extending the hips	Normal tone
Hearing loss		+	+
Congenital heart defect	−	−	+
Seizure/epilepsy		−	+
Central nervous system			
Cerebral atrophy	+	+	+
Craniofacial			
Triangular face	+	+	+
Hypertelorism	+	+	+
Hypoplastic alae nasi	+	+	+
Sparse hair	+		+
Down-slanting palpebral fissures	+		+
Long columella	+		+
Short, well-defined philtrum	+		+
Thin lips	+		+
Microretrognathia	+		+
Low-set ears	+		+
Extremities			
Arthrogryposis			+
Preaxial polydactyly			+
Clinodactyly of 5th fingers	+		+
Talipes equinovarus		+	
Talopes valgus			+
Ocular			
Retinal dysplasia			+
Microphthalmia		+	−
Duane anomaly		+	n.d.
Strabismus	+		−
Others			
Genital anomlies		+	−

Shadow indicates common features among three cases. y, year(s); m, month(s); +, positive; −, negative; n.d., not determined.

junction PCRs denied the deletion in parental samples (FISH data not shown and Fig. 2B by PCR using primers A, B, and C [primer B: 5′-AGC TGC TCA AAG TGG GGT ATT CTG G-3′]).

DISCUSSION

In this study, we precisely analyzed the 6.5-Mb deletion at 20q11.2–q12 in a boy, presenting with abnormal hands and feet, retinal dysplasia, and intractable feeding difficulty. Proximal interstitial deletions of 20q11–q12 are very rare. Only two cases have been reported and analyzed either by chromosomal CGH and FISH analysis or BAC array CGH with 1-Mb resolution [Callier et al., 2006; Iqbal and Al-Owain, 2007]. Clinical features are presented in Figure 1 and summarized in Table I. Three deletions are overlapping and the shortest region of overlap is from 20q11.22 to q11.23 (Fig. 3). Common clinical features among three cases are

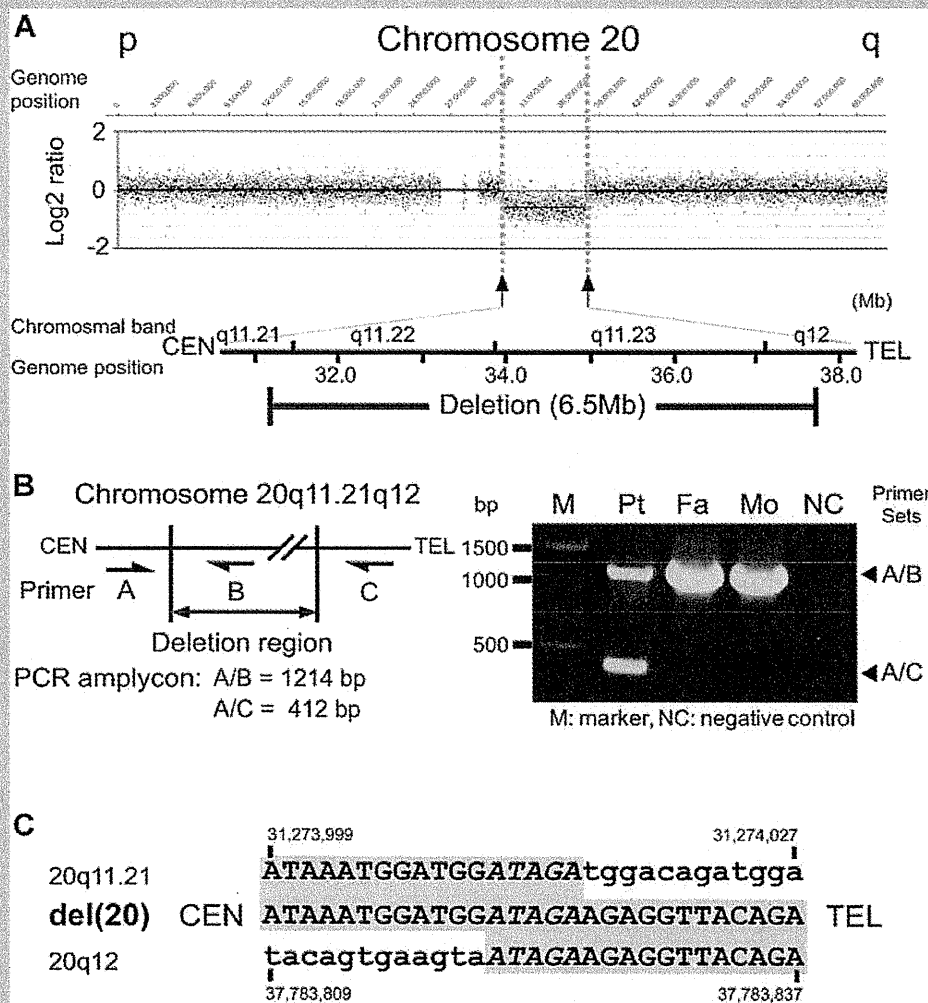

FIG. 2. Analysis of the 20q11.21–q12 deletion. A: High-resolution SNP array revealed the 6.5-Mb deletion at 20q11.21–q12. In the upper part, *Y* and *X* axes indicate probe signal intensity (log 2 ratio) and probe position in chromosome 20, respectively, and in the lower, chromosomal bands together with location of the deletion are shown. B: PCR system (left) to delineate the deletion and its result (right). C: Deletion junction sequence. Upper and lower sequences are normal ones around at proximal [20q11.21] and distal [20q12] deletion breakpoints, respectively. Middle shows the deletion junction in the patient. Gray shadow indicates matched sequences.

growth/developmental retardation, intractable feeding difficulties with GER, cerebral atrophy, and dysmorphic face including triangular face, hypertelorism, and hypoplastic alae nasi. In addition, two out of three patients shared many other facial dysmorphism including sparse hair, downslanting palpebral fissures, long columella, short and well-defined philtrum, thin lips, microretrognathia, and low-set ears. These findings suggest that the 20q11.22–q11.23 deletion can be a recognizable microdeletion syndrome. In addition, unique findings of hands and feet abnormalities as well as retinal dysplasia were found in our patient.

Intractable feeding difficulties in the three patients, is the largest concern for the family, and are speculated to be caused by combined factors: prolonged dysphagia (in our case), aspiration associated with GER (in all three), upper gastrointestinal tract abnormalties (pyloric stenosis [Callier et al., 2006] or esophageal hiatus hernia in our case), vomiting/diarrhea because of feeding intorerance [Callier et al., 2006], sensory abnormalities (in all), and food refusal (in the Callier et al. and our patient).

According to UCSC genome browser (March 2006 assembly), the 6.5-Mb deleted segment identified in our patient encompasses at least 96 known genes, including nine genes related to human disorders. One of these is growth/differentiation factor-5 (*GDF5*, also known as *CDMP1*). This is a protein which belongs to the GDF-subgroup of BMPs and plays an key regulatory role in embryonic skeletal and joint development. *GDF5* abnormalities are known to cause a variety of different skeletal disorders. Interestingly, Everman et al. [2002] and Yang et al. [2008] indicated that functional *GDF5* haploinsufficiency was the culprit of brachydactyly type C (BDC,

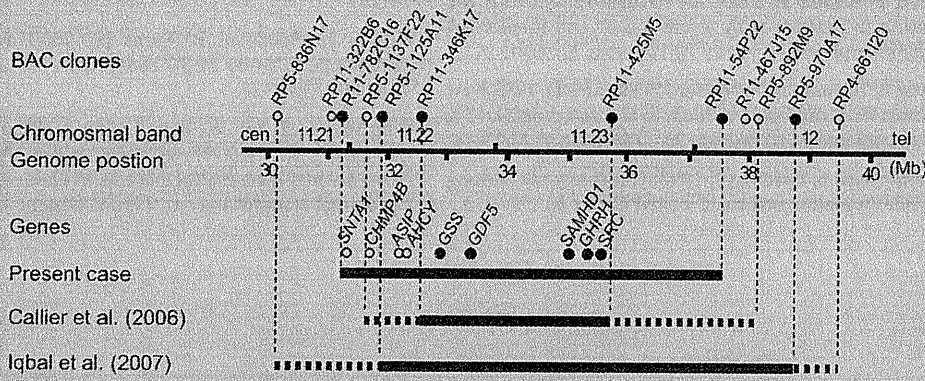

FIG. 3. Shematic presentation of the 20q11–q12 deletions. From top to bottom, BAC clones delineating deletions of all the cases (filled dot: deleted, open dot: not deleted) [Callier et al., 2006; Iqbal and Al-Owain, 2007], chromosomal bands from 20q11.2 to 20q12, genomic position, OMIM genes, and deleted regions of our case and previous ones. Solid and dotted horizontal lines indicate deleted and unconfirmed regions due to the relatively low resolution of the analytical methods.

OMIM #113100) by in vitro studies. As our patient has the *GDF5* haploinsufficiency, he may have the risk for BDC. However, he did not show this manifestation. He did have polydactyly, talipes valgus, and absence of the middle phalanges of the toes, which have been often found in individuals with BDC [Everman et al., 2002; Temtamy and Aglan, 2008]. Our patient did have a fetal akinesia (or hypokinesia) deformation phenotype (FADP). The short neck, hypertelorism, micrognathia, small thorax, postnatal respiratory disturbance, prolonged feeding difficulty, and slender long bone could represent FADP. FADP is a clinically and genetically heterogeneous constellation arising from fetal akinesia or decrease in utero movement due to intrinsic factors including neuropathy, myopathy, and restrictive dermopathy or extrinsic factors that limit fetal movement (e.g., tetragen exposure or fetal crowding) [Witters et al., 2002; Bamshad et al., 2009]. As extrinsic factors (e.g., abnormality of amniotic fluid, fetal crowding, congenital infection, and use of the drug in utero) could not be confirmed in this patient and the arthrogryposis and FADP are accompanied by other organ anomalies and developmental delay, the gene(s) at 20q11.21–q11.23 may be a primary intrinsic cause. Unfortunately, as skeletal malformations in the other two cases having the 20q11.2–q12 deletion were not fully described [Callier et al., 2006; Iqbal and Al-Owain, 2007], it is difficult to discuss the relationship between skeletal features and gene(s) in 20q11.2–q12 deletion.

Retinal dysplasia associated with falciform retinal fold and impaired vision was also noted. Retinal dysplasia is defined as abnormal growth and differentiation of embryonic retina either due to in utero environmental factors such as viral infection, tetragen exposure, retinopathy of prematurity or genetic factors. To our knowledge, this is the first description of retinal dysplasia associated with 20q11.2–q12 deletion.

ACKNOWLEDGMENTS

We are grateful to the patient and his family for their participation and support to this study. Grant-in Aid for Japan Society for the Promotion of Science (JSPS) Fellow (A.N.), Research Grants from the Ministry of Health, Labour and Welfare (N.M.), Grant-in-Aid from the Ministry of Education, Culture, Sports, Science and Technology of Japan (N.M.), and Grant-in-Aid for Scientific Research from JSPS (N.M.).

REFERENCES

Aldred MA, Aftimos S, Hall C, Waters KS, Thakker RV, Trembath RC, Brueton L. 2002. Constitutional deletion of chromosome 20q in two patients affected with albright hereditary osteodystrophy. Am J Med Genet 113:167–172.

Bamshad M, Van Heest AE, Pleasure D. 2009. Arthrogryposis: A review and update. J Bone Joint Surg Am 91:40–46.

Borozdin W, Graham JM Jr, Bohm D, Bamshad MJ, Spranger S, Burke L, Leipoldt M, Kohlhase J. 2007. Multigene deletions on chromosome 20q13.13-q13.2 including SALL4 result in an expanded phenotype of Okihiro syndrome plus developmental delay. Hum Mutat 28:830.

Callier P, Faivre L, Marle N, Thauvin-Robinet C, Sanlaville D, Gosset P, Prieur M, Labenne M, Huet F, Mugneret F. 2006. Major feeding difficulties in the first reported case of interstitial 20q11.22-q12 microdeletion and molecular cytogenetic characterization. Am J Med Genet Part A 140A:1859–1863.

Everman DB, Bartels CF, Yang Y, Yanamandra N, Goodman FR, Mendoza-Londono JR, Savarirayan R, White SM, Graham JM Jr, Gale RP, Svarch E, Newman WG, Kleckers AR, Francomano CA, Govindaiah V, Singh L, Morrison S, Thomas JT, Warman ML. 2002. The mutational spectrum of brachydactyly type C. Am J Med Genet 112:291–296.

Genevieve D, Sanlaville D, Faivre L, Kottler ML, Jambou M, Gosset P, Boustani-Samara D, Pinto G, Ozilou C, Abeguile G, Munnich A, Romana S, Raoul O, Cormier-Daire V, Vekemans M. 2005. Paternal deletion of the GNAS imprinted locus (including Gnasxl) in two girls presenting with severe pre- and post-natal growth retardation and intractable feeding difficulties. Eur J Hum Genet 13:1033–1039.

Iqbal MA, Al-Owain M. 2007. Interstitial del(20)(q11.2q12)—Clinical and molecular cytogenetic characterization. Am J Med Genet Part A 143A:1880–1884.

Kanda T, Murayama K, Kondo I, Kitazumi E, Takahashi K, Nakatani K, Yoneyama A, Yamori Y, Kanda Y. 2005. An estimation chart for the possibility of aspiration in patients with severe motor and intellectual disabilities: Its reliability and accuracy. No To Hattatsu 37:307–316.

Petersen MB, Tranebjaerg L, Tommerup N, Nygaard P, Edwards H. 1987. New assignment of the adenosine deaminase gene locus to chromosome 20q13 X 11 by study of a patient with interstitial deletion 20q. J Med Genet 24:93–96.

Shabtai F, Ben-Sasson E, Arieli S, Grinblat J. 1993. Chromosome 20 long arm deletion in an elderly malformed man. J Med Genet 30:171–173.

Temtamy SA, Aglan MS. 2008. Brachydactyly. Orphanet J Rare Dis 3:15.

Witters I, Moerman P, Fryns JP. 2002. Fetal akinesia deformation sequence: A study of 30 consecutive in utero diagnoses. Am J Med Genet 113:23–28.

Yang W, Cao L, Liu W, Jiang L, Sun M, Zhang D, Wang S, Lo WH, Luo Y, Zhang X. 2008. Novel point mutations in GDF5 associated with two distinct limb malformations in Chinese: Brachydactyly type C and proximal symphalangism. J Hum Genet 53:368–374.

RESEARCH ARTICLE

AMERICAN JOURNAL OF medical genetics PART A

Axenfeld–Rieger Anomaly and Axenfeld–Rieger Syndrome: Clinical, Molecular-Cytogenetic, and DNA Array Analyses of Three Patients With Chromosomal Defects at 6p25

Hidefumi Tonoki,[1,2]* Naoki Harada,[3] Osamu Shimokawa,[3] Ayako Yosozumi,[2] Kadomi Monzaki,[2] Kohei Satoh,[4] Rika Kosaki,[5] Atsushi Sato,[6] Naomichi Matsumoto,[7] and Susumu Iizuka[1]

[1]Section of Clinical Genetics, Department of Pediatrics, Tenshi Hospital, Sapporo, Japan

[2]Department of Pediatrics, Hokkaido University Graduate School of Medicine, Sapporo, Japan

[3]Kyushu Medical Science Nagasaki Laboratory, Nagasaki, Japan

[4]Department of Pediatrics, Sapporo Kousei Hospital, Sapporo, Japan

[5]Department of Clinical Genetics and Molecular Medicine, National Center for Child Health and Development, Okura, Setagaya-ku, Tokyo, Japan

[6]Faculty of Medicine, Department of Pediatrics, The University of Tokyo, Hongo, Bunkyo-ku, Tokyo, Japan

[7]Department of Human Genetics, Yokohama City University Graduate School of Medicine, Fukuura, Kanazawa-ku, Yokohama, Japan

Received 1 March 2010; Accepted 29 November 2010

Clinical phenotypes of and genetic aberrations in three unrelated Japanese patients with Axenfeld–Rieger anomalies and various accompanying malformations of systemic organs are described. GTG-banded chromosome analysis showed terminal deletions of the short arm of chromosome 6 in two patients and an inversion, inv(6)(p25q14), in the other. FISH and DNA array analyses revealed that the two patients with deletions had 5.0–5.7 Mb and 6.6 Mb 6p terminal deletions, respectively, and *FOXC1* was apparently deleted in both patients. In the other patient, the inversion breakpoint at 6p25 was estimated to be in or very close to the *FOXC1* locus, but DNA array analysis did not reveal a deletion around the breakpoint. Common extraocular findings in these patients included broad forehead, brachycephaly, hypertelorism, downslanting palpebral fissures, small anteverted nose, and cardiac defects. Two patients also exhibited autistic characteristics. The two patients with deletions exhibited poor muscle tone and developmental delays. Most of these extraocular findings were similar to those found in previous patients with *FOXC1* mutations and distinct from those found in patients with *PITX2* mutations, who frequently develop umbilical and dental anomalies. We suggest that the psychomotor retardation is a clinical manifestation associated with a deletion of multiple contiguous genes in the 6p terminus and that this phenomenon is similar to the 6p25 deletion syndrome. Understanding the relationship between genetic lesions and the spectrum of extraocular findings in patients with Axenfeld–Rieger anomalies may lead to better clinical management. © 2011 Wiley Periodicals, Inc.

Key words: Axenfeld–Rieger anomaly; FOXC1; PITX2; DNA array; FISH; Rieger syndrome

How to Cite this Article:
Tonoki H, Harada N, Shimokawa O, Yosozumi A, Monzaki K, Satoh K, Kosaki R, Sato A, Matsumoto N, Iizuka S. 2011. Axenfeld–Rieger anomaly and Axenfeld–Rieger syndrome: Clinical, molecular-cytogenetic, and DNA array analyses of three patients with chromosomal defects at 6p25.
Am J Med Genet Part A 155:2925–2932.

INTRODUCTION

Axenfeld–Rieger anomalies, a group of genetically and phenotypically heterogeneous disorders leading to aberrant development of the anterior eye chambers, are frequently accompanied by a variety of major and minor anomalies of systemic organs, and patients with Axenfeld–Rieger anomalies have a 50% or higher incidence of

*Correspondence to:
Hidefumi Tonoki, M.D., Ph.D., Section of Clinical Genetics, Department of Pediatrics, Tenshi Hospital N-12, E-3, Sapporo 064-8611, Japan.
E-mail: hidefumi.tonoki@tenshi.or.jp
Published online 18 October 2011 in Wiley Online Library (wileyonlinelibrary.com).
DOI 10.1002/ajmg.a.33858

© 2011 Wiley Periodicals, Inc.

glaucoma [Fitch and Kaback, 1978; Alward, 2000]. Genetic loci associated with Axenfeld–Rieger anomalies have been mapped to three chromosomal regions: 4q25, 6p25, and 13q14 [Mears et al., 1996; Phillips et al., 1996; Semina et al., 1996a]. While the gene at 13q14 has not been identified, it is known that mutations in *PITX2* cause Axenfeld–Rieger anomalies mapping to 4q25 [Semina et al., 1996b] and that mutations in *FOXC1* underlie Axenfeld–Rieger anomalies mapping to 6p25 [Mears et al., 1998; Nishimura et al., 1998].

Historically, Axenfeld–Rieger anomalies and related conditions have been classified as Axenfeld anomaly, Rieger anomaly, or Rieger syndrome. Patients were considered to have Axenfeld anomaly when they presented with iris strands connecting the iridocorneal angel to the trabecular meshwork and a prominent, anteriorly displaced Schwalbe's line (posterior embryotoxon). If those patients presented with iris hypoplasia, corectopia (abnormal situation of pupil), or polycoria, they were considered to have Rieger anomaly. When these ocular findings were concurrent with facial, dental, or umbilical defects, patients were considered to have Rieger syndrome. However, the overlap in the spectrum of clinical manifestations and genetic heterogeneity in these patients makes this classification scheme somewhat confusing and has led to the proposal that these defects be classified as Axenfeld–Rieger anomaly (ARA) for patients presenting ocular defects only and Axenfeld–Rieger syndrome for patients with ocular and extraocular defects [Shields, 1983]. The term Axenfeld–Rieger anomalies is used to describe ARA with or without extraocular defects [Lines et al., 2002], but the correlation between the clinical and genetic findings in the subsets of patients has not been clearly established.

Here, we describe the clinical phenotypes of and genetic aberrations in three Japanese patients with ARA. Separate terminal deletions of chromosome 6p were found in two patients with phenotypes characteristic of so called Axenfeld–Rieger syndrome. The other patient who had congenial glaucoma and Rieger anomaly visited us asking whether his ocular anomaly was related to his abnormal karyotype: 46,XY,inv(6)(p25.1q12.1),t(4;12)(p25;q14).

CLINICAL REPORTS

This project was approved by the Committee for genetic test and counseling, Tenshi Hospital, Japan.

Patients

Patient 1. This Japanese girl was born after 42 weeks of gestation with a birth weight of 2,258 g (<5th centile), length of 47.4 cm (32nd centile), and head circumference of 33.0 cm (47th centile) to unrelated Japanese parents, who were both phenotypically normal.

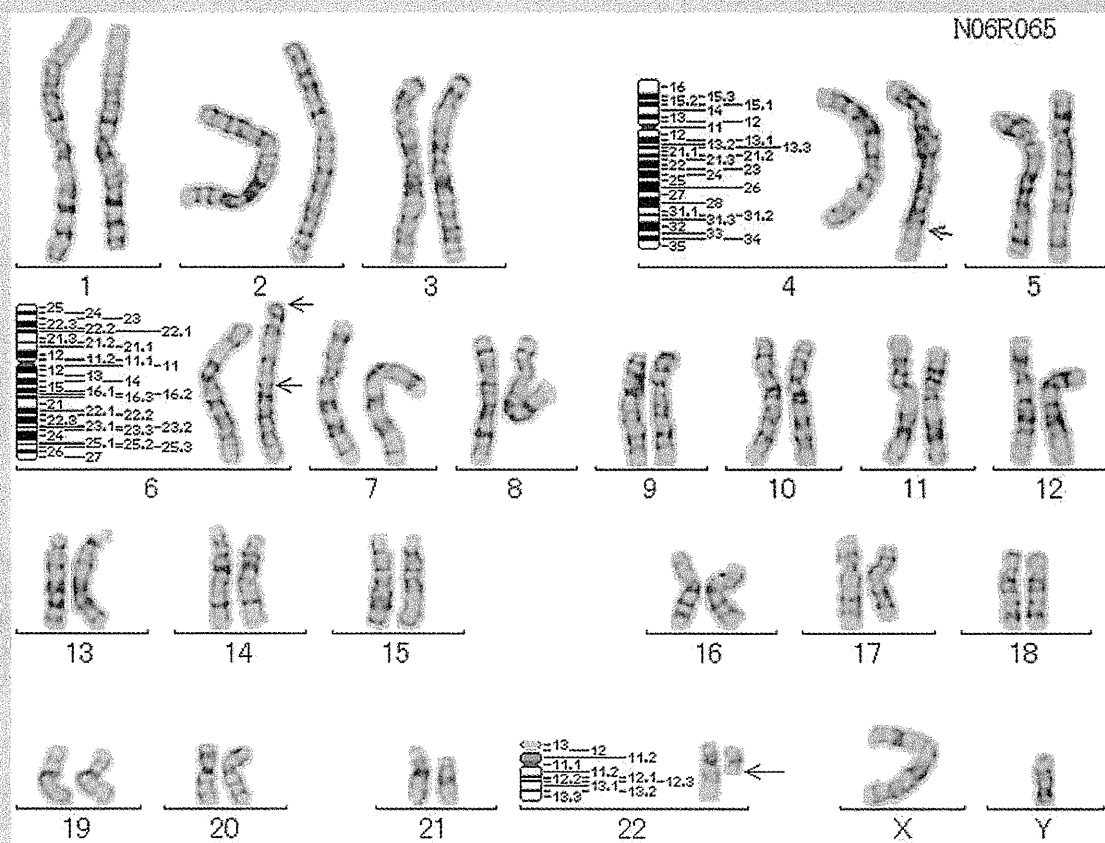

FIG. 1. GTG-banded chromosomes of Patient 2, whose karyotype was 46,XY,inv(6)(p25q14),t(4;22)(q35;q11.1).

She exhibited a number of congenital anomalies, including apparent hypertelorism, downslanting palpebral fissures, high palate, fusion of labia minor, redundant peri-umbilical skin, agenesis of corpus callosum, atrial septal defect, and bilateral sensorineural deafness. Ocular findings included buphthalmos in the neonatal period, posterior embryotoxon, and strabismus. Her intraocular pressure and pupil shape were normal, leading to a diagnosis of Axenfeld anomaly. Her developmental milestones were delayed; she controlled her head at 4 months of age, sat without support at 11 months, walked at 22 months, and had not spoken any meaningful words at 24 months. When measured at 19 months of age, her height was 80.2 cm (49th centile) and weight was 9.2 kg (21st centile). She showed autistic behavior at 5 years of age.

Standard G-banded chromosome analysis and multiple-chromosome painting revealed 46,XX,del(6)(p25.1). The karyotypes of the parents were normal.

Patient 2. This Japanese boy was born after 37 weeks of gestation with a weight of 2,926 g (64th centile), length of 48.0 cm (45th centile), and head circumference of 34.0 cm (62nd centile) to unrelated Japanese parents, who were phenotypically normal. In the neonatal period, he presented with cloudy cornea. Ophthalmological examination revealed that he had increased intraocular pressure, posterior embryotoxon, and iridogoniodysgenesis, leading to a diagnosis of Rieger anomaly. Chromosomal analysis showed an abnormal karyotype: 46,XY,inv(6)(p25q14),t(4;22)(q35;q11.1) (Fig. 1). When he visited us for genetic counseling at age 14 months he had a broad forehead and brachycephaly, apparent hypertelorism, downslanting palpebral fissures, maxillar hypoplasia, a small anteverted nose, and aortic coarctation. Dental, otic, or umbilical anomalies were not found. Audiologic examination did not reveal a hearing defect. Brain CT examination and ultrasound screening for abdominal organs were both normal. By the age of 2 years, he had undergone trabeculotomy and trabeculectomy on both eyes several times to control intraocular pressure. His growth and development were normal. He showed autistic behavior at 3 years of age. G-banded chromosomal analyses of the parents were normal.

Patient 3. This Japanese boy was born after 40 weeks of gestation with a birth weight of 3,230 g (56th centile), length of 49.1 cm (39th centile), and head circumference of 32.5 cm (28th centile) to unrelated Japanese parents, who were phenotypically normal. Atrial septal defect and pulmonary stenosis were found in the neonatal period, but no treatment was needed. Buphthalmos was noticed at 4 months of age. Ophthalmological examination revealed increased intraocular pressure and posterior embryotoxon. He was referred to us for genetic counseling at 8 months. He had a broad forehead, apparent hypertelorism, downslanting palpebral fissures, low-set and malformed ears, and a small anteverted nose. Brain MRI and brainstem auditory evoked potential were normal. No dental or umbilical anomalies were found. No surgery was necessary to treat the increased intraocular pressure. He was hypotonic, and his development was mildly delayed. His growth was normal. Chromosomal analysis revealed an abnormal karyotype: 46,XY,der(6)t(X;6)(p22.3;p25)dn. or 46,XY,der(6)t-(Y;6)(p22.3;p25)dn. The karyotypes of the parents were normal.

METHODS

Chromosomal analysis was performed on peripheral blood lymphocytes. Metaphase chromosomes were G-banded for karyotype analysis and prepared for fluorescence in situ hybridization (FISH) analysis. RP-11 human BAC clones that map near the 6p25 breakpoints and the distal part of 6p were selected and utilized for FISH analysis, which was performed according to the standard protocol [Shimokawa et al., 2005]. Mapping information was retrieved from the UCSC genome browser, 2004 May version

TABLE I. FISH Results of Patients 1 and 2

		Position		FISH result	
Clone name	Band	Start	End	Patient 1	Patient 2
GS-62I11	6p25.3	Subtelomeric clone		Deletion	
RP11-139J12	6p25.3	74360	251686	Deletion	
RP11-939G22	6p25.3	924064	1099477	Deletion	Normal
RP11-10501	6p25.3	1099176	1279132		Normal
RP11-140F23	6p25.3	1304215	1456195		Normal
RP11-157J24	6p25.3	1372372	1547233		Normal
RP11-205J13	6p25.3	1456202	1625486	Deletion	Split
RP11-13F18	6p25.3	1462376	1633119		Split
RP11-964J7	6p25.3	1499784	1698745		Split
RP11-265E5	6p25.3	1562987	1723184		Inverted
RP11-452I2	6p25.3	1973365	2159947	Deletion	Inverted
RP11-420G6	6p25.2	2641239	2815840	Deletion	
RP11-349H3	6p25.1	4800266	4978093	Deletion	
RP11-324B14	6p25.1	5789659	5942278	Normal	
RP11-796J17	6p25.1	6331029	6531292	Normal	
RP11-69L16	6p24.3	7184568	7351773	Normal	
RP11-1065N24	6p24.2	11190385	11284706	Normal	

(http://genome.ucsc.edu/cga-bin/hgGateway). We also performed DNA array examination with Affymetrix GeneChip 250K Nsp array of 263,000 SNPs according to the manufacruer's protocols, and the data were analyzed using CNAG 3.0 software.

RESULTS

In Patient 1, FISH analyses using BAC clones, GS-62I11 (6p25.3), RP11-139J12 (6p25.3), RP11-939G22 (6p25.3), RP11-205J13 (6p25.3) (which encompasses the *FOXC1* gene), RP11-452I2 (6p25.3), RP11-452I2 (6p25.2), RP11-420G6 (6p25.2), and RP11-349H3 (6p25.1) resulted in a single spot of fluorescence. In contrast, hybridization with clones RP11-324B14 (6p25.1), RP11-796J17 (6p25.1), RP11-69L16 (6p24.3), and RP11-1065N24 (6p24.2) resulted in two fluorescent signals (Table I and Fig. 2). These results were confirmed by a comparative genomic hybridization study that revealed a 5.0–5.7 Mb 6p terminal deletion (data not shown).

In Patient 2, three *FOXC1*-containing clones, RP11-205J13, RP11-13F18, and RP11-265E5, gave split signals on the inv(6)chromosome, while clones distal and proximal to *FOXC1* gave signals at the original position and at the inverted position, respectively (Table I and Fig. 2). DNA array analysis revealed no loss or gain of signals on any part of chromosomes 6 (Fig. 3a), 4, or 22 (data not shown).

In Patient 3, DNA array tests revealed a 6,610 kb deletion of the short arm of chromosome 6 encompassing SNP A-2058596 (position 119,769) to SNP A-1892272 (position 6,735,864) (Fig. 3b).

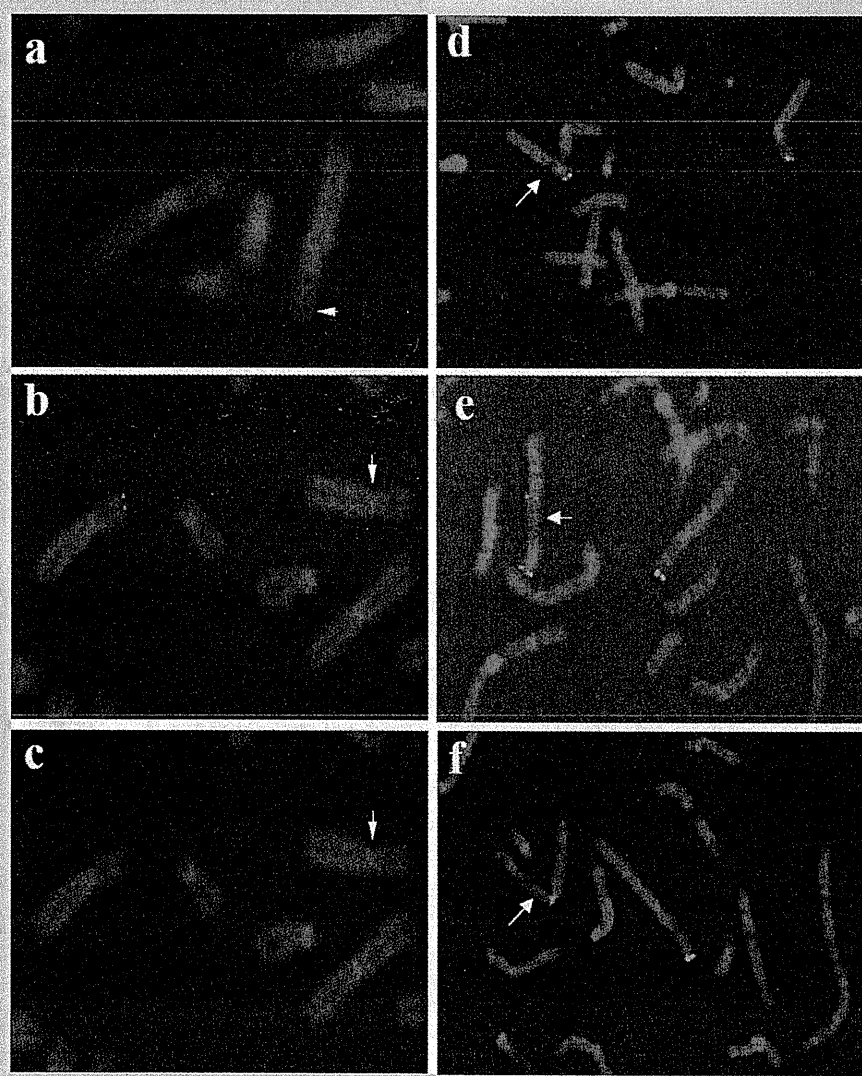

FIG. 2. FISH analysis of Patient 1 with BAC clones. RP11-205J13 on 6p25.3 (a) and clone RP11-349H3 on 6p25.1 (b) did not give any signal on del(6)(arrow). RP11-324B14 (c) on 6p25.1 gave a signal on del(6) (arrow). FISH analysis of Patient 2 (d,e), with BAC clones RP11-157J24 (d), RP11-13F18 (e), and RP11-265E5 (f), showing distal, split, and proximal (inverted position) signals, respectively, on inv(6). [Color figure can be seen in the online version of this article, available at http://onlinelibrary.wiley.com/journal/10.1002/(ISSN)1552-4833]

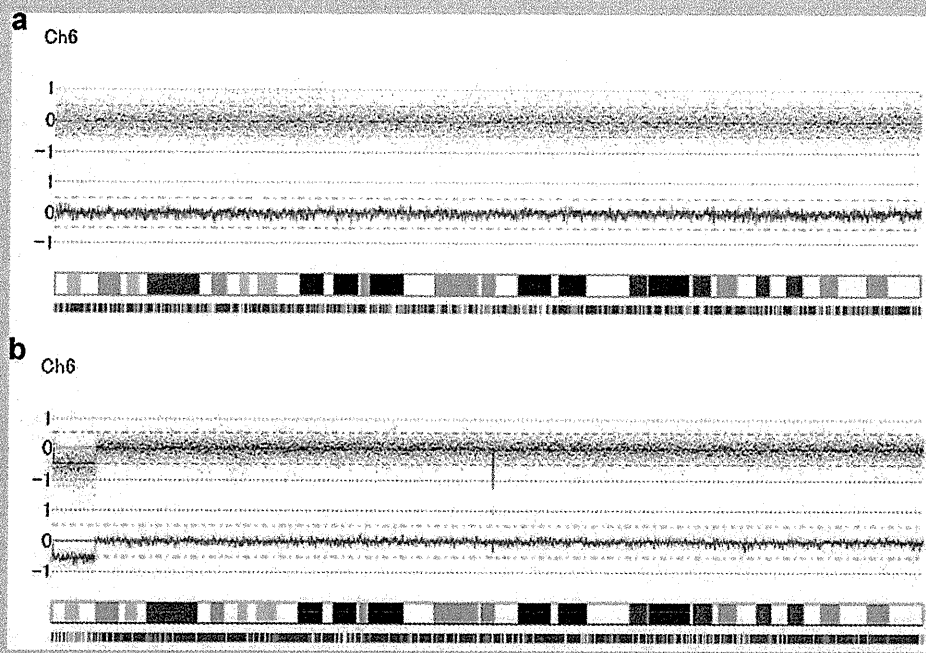

FIG. 3. DNA array examination with Affymetrix mapping 250K array for 263,000 SNPs in Patients 2 and 3. These data were analyzed using GTC and CNAG software, revealing no loss or gain of signals of chromosome 6 in Patient 2 (a) and 6.61 kb deletion of terminal region of the short arm of chromosome 6 in Patient 3 (b). [Color figure can be seen in the online version of this article, available at http://onlinelibrary.wiley.com/journal/10.1002/(ISSN)1552-4833]

DISCUSSION

We analyzed the genomic lesions in three patients with ARA. The FISH analyses and DNA array examinations along with G-banded chromosome analyses clearly showed a 5.0–5.7 Mb and a 6.6 Mb 6p terminal deletion in Patients 1 and 3, respectively (Fig. 4). *FOXC1* coding sequence is located at position 1555680–1557341 in 6p25.3, and the gene was apparently deleted both in Patients 1 and 3. In Patient 2, the results of FISH analyses and DNA array examination indicated that the chromosomal breakpoint at 6p25.3 was in or very close to the *FOXC1* locus (Fig. 4). Therefore, it is plausible that in Patient 2 the breakpoint at 6p25.3 directly interrupted the gene structure or somehow impaired the function of *FOXC1* through a position effect, similar to that in a patient with a balanced translocation, t(6;13)(p25.3;q22.3) [Nishimura et al., 1998].

Several patients with 6p terminal deletions have been reported [Kume et al., 1998; Law et al., 1998; Nishimura et al., 1998; Baruch and Erickson, 2001; Lehmann et al., 2002; Anderlid et al., 2003; Maclean et al., 2005; Suzuki et al., 2006; Martinez-Glez et al., 2007; Martinet et al., 2008]. Recently, Gould et al. [2004] and Lin et al. [2005] summarized the phenotypes of patients with 6p25 deletions, showing that these patients exhibited a recognizable pattern of malformations, namely 6p25 deletion syndrome. These malformations include hypertelorism, downslanting palpebral fissures, ARA, hearing loss, anomalies in the central nervous system, and developmental delay. As shown in Table II, manifestations of Patients 1 and 3 were consistent with those of the 6p25 deletion

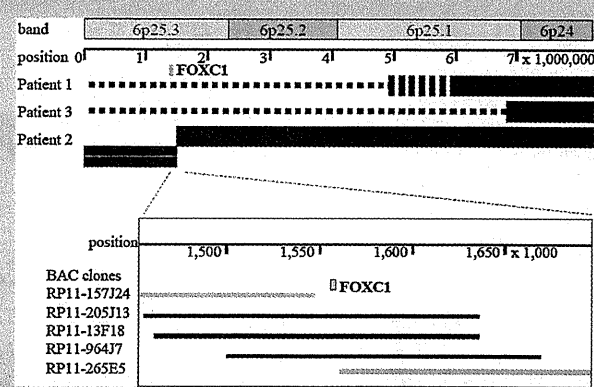

FIG. 4. Diagram of the chromosomal aberrations in Patients 1, 2, and 3. The dotted bars indicate the extent of the 6p terminal deletions in Patients 1 and 3. In Patient 2, slippage of the boxes indicates the breakpoint. In the lower box, locations of *FOXC1* and some of the BAC clones used to analyze samples from Patient 2 are shown. *FOXC1* is located between BAC clones RP11-157J24 and RP11-265E5, which gave the signals at the normal and inverted position, respectively, on Inv(6). Three BAC clones that gave split signals on Inv(6) overlap each other and contain *FOXC1*.

TABLE II. Summary of Clinical Findings in Patients With 6p25 Anomalies

	This report			Nishimura et al.	Gould et al.	Lin et al.
	P1	P3	P2	First patient	19 cases	9 cases[b]
	6p25 deletion					
Chromosomal anomaly[a]			Inv	TB	6p25 deletion	6p25 deletion
Anterior chamber defect	+	+	+	+	17/19	7/9
Broad forehead and brachycephaly	+	+	+			
Hypertelorism	+	+	+	+	12/14	7/8
Downslanting palpebral fissures	+	+	+			6/7
Small/anteverted nose	+	+	+			
Palatal anomaly	+	−	−	+		
Dental anomalies	−	−	−			
Ear anomalies	−	+	−			4/8
Hearing loss	+	−	−		14/15	6/8
Umbilical anomalies	+	−	−			1/4
Structural CNS anomaly	+	−	−	+	8/14	3/5
Cardiac defects	+	+	+		9/14	6/8
Hypoplastic lungs	−	−	−	+		
Genitourinary anomaly	+	−	−			1/2
Poor muscle tone	+	+	−			3/4
Developmental delay	+	+	−			9/9

P2, Patient 2; P3, Patient 3; P1, Patient 1 in this report.
+, present; −, not present; blank, not reported.
[a]Inv inv(6)(p25q14), TB: t(6;13)(p25.3;q22.3).
[b]Three cases were also reviewed by Gould et al.

syndrome. Most of the clinical manifestations in these patients were thought to be due to haploinsufficiency of multiple genes in the 6p terminal region. Patient 2 in this study and a patient reported by Nishimura et al. [1998] each had a balanced chromosomal rearrangement and exhibited diverse multiple extraocular findings; for example, Patient 2 exhibited apparent hypertelorism, downslanting of palpebral fissures, maxillar hypoplasia, and aortic coarctation, while the patient from the previous report exhibited hypertelorism, palatal anomaly, CNS anomaly, and hypoplastic lungs. The diversity of these phenotypes suggests that chromosome breakage at

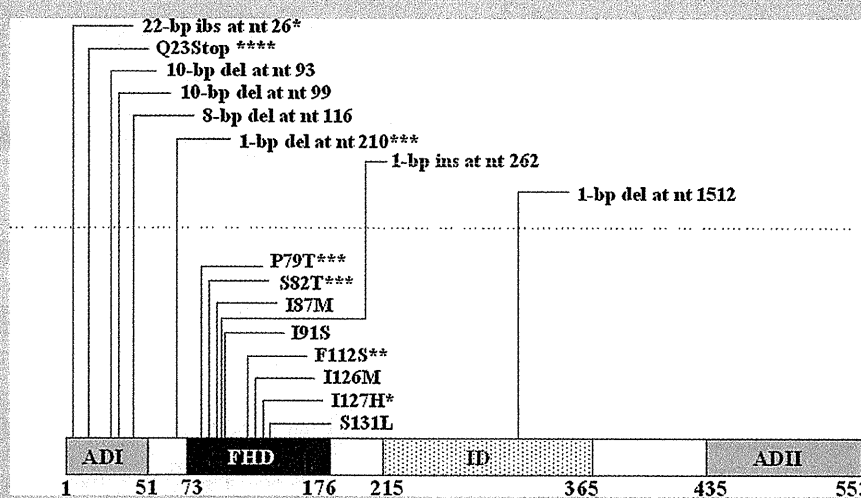

FIG. 5. Schematic representation of previously reported *FOXC1* mutations and associated phenotypes. Boxes represent FOXC1 domains, and the numbers indicate amino acid positions. ADI, activation domain I; FHD, forkhead domain; ID, inhibitory domain; and ADII, activation domain II. The truncation mutations are above dotted line, and the missense mutations are below it. Symbols on the right shoulder of mutation indicate that patients carrying the mutation had the following extraocular findings: *, hypertelorism; **, dental anomaly; ***, cardiac anomaly; ****, hypertelorism and dental, umbilical, and cardiac anomalies.